Army Research Laboratory

The Effects of Layer Constraint on Stress Wave Propagation in Multilayer Composite Materials

by Alper Tasdemirci, Ian W. Hall, Bazle A. Gama, and Mustafa Guden

ARL-CR-550 **September 2004**

prepared by

Department of Mechanical Engineering
University of Delaware
Center for Composite Materials
Newark, DE 19716

under contract

DAAD19-01-2-0001

NOTICES

Disclaimers

Army Research Laboratory

Aberdeen Proving Ground, MD 21005-5069

ARL-CR-550 **September 2004**

The Effects of Layer Constraint on Stress Wave Propagation in Multilayer Composite Materials

Alper Tasdemirci, Ian W. Hall, and Bazle A. Gama
Department of Mechanical Engineering and
Center for Composite Materials
University of Delaware

Mustafa Guden
Department of Mechanical Engineering,
Izmir Institute of Technology

prepared by

Department of Mechanical Engineering
University of Delaware
Center for Composite Materials
Newark, DE 19716

under contract

DAAD19-01-2-0001

Report Documentation Page	*Form Approved* *OMB No. 0704-0188*

1. REPORT DATE *(DD-MM-YYYY)*	2. REPORT TYPE	3. DATES COVERED (From - To)
September 2004	Final	September 2003

4. TITLE AND SUBTITLE
The Effects of Layer Constraint on Stress Wave Propagation in Multilayer Composite Materials

5a. CONTRACT NUMBER DAAD19-01-2-0001
5b. GRANT NUMBER
5c. PROGRAM ELEMENT NUMBER

6. AUTHOR(S)
Alper Tasdemirci,* Ian W. Hall,* Bazle A. Gama,* and Mustafa Guden†

5d. PROJECT NUMBER 622618.AH80
5e. TASK NUMBER
5f. WORK UNIT NUMBER

7. PERFORMING ORGANIZATION NAME(S) AND ADDRESS(ES)
University of Delaware
Department of Mechanical Engineering
Center for Composite Materials
Newark, DE 19716

8. PERFORMING ORGANIZATION REPORT NUMBER

9. SPONSORING/MONITORING AGENCY NAME(S) AND ADDRESS(ES)
U.S. Army Research Laboratory
ATTN: AMSRD-ARL-WM-MB
Aberdeen Proving Ground, MD 21005-5066

10. SPONSOR/MONITOR'S ACRONYM(S) ARL-CR-550
11. SPONSOR/MONITOR'S REPORT NUMBER(S)

12. DISTRIBUTION/AVAILABILITY STATEMENT
Approved for public release; distribution is unlimited.

13. SUPPLEMENTARY NOTES
*Department of Mechanical Engineering and Center for Composite Materials, University of Delaware, Newark, DE 19716
†Department of Mechanical Engineering, Izmir Institute of Technology, Izmir, Gulbahce, Turkey

14. ABSTRACT
Multilayer materials consisting of ceramic and glass/epoxy with a rubber interlayer have been subjected to a high strain rate compression using a split-Hopkinson Pressure Bar (SHPB). The feasibility of modeling stress wave propagation in complex multilayer materials has been demonstrated. It has been shown that the effects of lateral confinement of a normally low-modulus interlayer material can significantly affect the response to wave propagation.

Numerical modeling clearly shows that severe stress inhomogeneities and discontinuities exist, and these may have serious consequences for the mechanical and other properties. The one-dimensional stress state usually assumed for conventional SHPB testing is therefore inapplicable, and both numerical and experimental results have to be coupled for a complete understanding of the wave propagation characteristics. In this study, both methods were used, and the stress states inside the components were presented.

15. SUBJECT TERMS
multilayer structures, finite element analysis, mechanical properties, high strain rate

16. SECURITY CLASSIFICATION OF:			17. LIMITATION OF ABSTRACT	18. NUMBER OF PAGES	19a. NAME OF RESPONSIBLE PERSON
					Alper Tasdemirci
a. REPORT	b. ABSTRACT	c. THIS PAGE			19b. TELEPHONE NUMBER (*Include area code*)
UNCLASSIFIED	UNCLASSIFIED	UNCLASSIFIED	UL	44	302-831-8850

Standard Form 298 (Rev. 8/98)
Prescribed by ANSI Std. Z39.18

Contents

List of Figures

List of Tables

Acknowledgments

The authors gratefully acknowledge financial support for this research under the Composite Materials Research Collaborative Program sponsored by the U.S. Army Research Laboratory, contract number DAAD19-01-2-0001.

INTENTIONALLY LEFT BLANK.

1. Introduction

Thick-section composite materials are frequently used under dynamic loading conditions, but their behavior is still not clearly understood. Impact loading of monolithic laminates has been the subject of several investigations, e.g., with glass/epoxy and graphite/epoxy (*1–10*). Similarly the penetration or perforation of composites has also been studied (*11*, *12*), but severe complications arose whenever widely dissimilar materials well in intimate contact because their differing impedances caused complex wave reflection and transmission phenomena at each interface encountered. Thick, layered, or graded structures have significant potential for armor applications, and Li et al. (*13*) reported the dynamic characterization of layered and graded structures under impulsive loading. Another example of multilayer materials is provided by modern integral composite armor for vehicle applications as described by Fink (*14*) and Gama et al. (*15–17*). The armor material must provide ballistic protection at minimum weight and may contain several layers of different impedance, usually a ceramic layer followed by a thick composite plate (e.g., glass fiber/epoxy). High-velocity impact of this type of integral armor has been the subject of finite element studies by Mahfuz et al. (*18*). Jovicic et al. (*19*) modeled the ballistic behavior of gradient design composite armors.

The elastic adhesives used in composite armors can also alter wave propagation in the armor components. The mechanical behavior of different elastic adhesives under impact loads was studied by Martinez et al. (*20*) who reported that the capability of transmitting and reflecting the impact energy depends on the thickness and the type of the adhesive used. They concluded that the utilization of a thin layer of a rigid adhesive was the best way to transmit energy with the lowest reflection coefficient.

A central concept in enhancing the ability of multilayer material structures to withstand rapid impulsive loading is to spread the local impact load as rapidly and widely as possible. This can be achieved by placing a high wave-speed layer in the layered system. Gupta and Ding (*21*) studied numerically the effects of wave speed, layering geometry, and mechanical properties of the layer and substrate on load spreading. They showed that for a fixed layer thickness, a single thick high-strength high wave-speed layer appears to be able to offer the best lateral load spreading through intense and rapid wave transmission and spreading. The low wave-speed material used in multilayered targets appears to deteriorate the load spreading capability of the layered system.

Design of efficient multilayer materials for impact resistance requires both modeling and experimental efforts, and the split-Hopkinson pressure bar (SHPB) is a convenient tool in the latter respect although conventional data reduction routines obviously cannot be used for these materials. Two- and three-dimensional (2-D and 3-D) wave propagation in Hopkinson bar tests has been investigated numerically by several authors (*22*, *23*). In experimental studies, impact velocity of the striker bar and axial strain on the bar surfaces are the most commonly measured quantities. In numerical studies, besides the parameters previously mentioned, displacement and velocity of nodes, strain and stress of the elements, and interface forces can all be acquired as a function of time (*24*).

Prior work (*25*) addressed the situation with three different layers consisting of ceramic, rubber and composite, in which lateral expansion of the rubber was permitted. However, in practical large-scale structures, the rubber interlayer would be constrained by the surrounding material, and this present report considers the effects of such lateral constraint on the resulting properties. Samples used in SHPB testing can, at the most, have the same diameter as the bar, and earlier experiments showed that considerable radial flow occurred in the rubber interlayer. Larger samples, typical of many anticipated applications, would be subjected to severe lateral constraints which would, in turn, affect the through-thickness stresses reported. In fact, the real case will probably lie somewhere between the extremes of completely constrained and completely unconstrained interlayers, so the evaluation of both limiting cases is correspondingly important.

The effect of lateral constraint on ballistic performance has been investigated by many authors, and it is now well known that a compressive prestress is helpful in improving the fracture energy and impact resistance in brittle materials. Espinosa et al. (*26*) experimentally studied the impact resistance of ceramics confined in steel fixtures and showed the enhancement of ballistic efficiency of the confined ceramics. Martinez et al. (*20*) have determined the stress-strain curve of confined adhesive used in armor at high strain rates. Within the armor, elastic adhesives, comparable with the rubber interlayer in our case, were used to bond two large plates of much more rigid materials, which themselves impede subsequent lateral displacements of the adhesive.

This study, then, presents the initial results of a combined experimental and numerical investigation and serves to delineate the principal features and identify the problems to be solved in order to develop a better understanding of the effects of constraint in such multilayer materials.

2. Experiments and Modeling

Samples were prepared from multilayer plates with layers of widely different impedances. The plates consisted of three layers, namely a 13.96-mm-thick alumina ceramic, a 1.5-mm-thick layer of ethylene propylene diene monomer (EPDM) rubber, and a layer of glass/epoxy composite.

The 5 × 5 plain weave S-2 Glass[*] fiber woven fabric (0.814 kg/m^2) SC15[†] epoxy (toughened resin) composite plates were 11.3-mm-thick and were produced using the vacuum-assisted resin transfer molding process. Lateral confinement of the rubber interlayer was obtained by placing a 6-mm-wide steel retaining ring around the junction of the sample as illustrated in figure 1. An interference fit was achieved between the rubber and the steel ring, and no rubber was squeezed out into the region between them while testing. Possible inertial effects and interactions between the ring and the other components of the sample were checked via tests on individual ceramic and composite samples with the ring in place. No modification to the wave propagation behavior was observed in the presence of the steel ring. The ceramic layer was always at the impacted side.

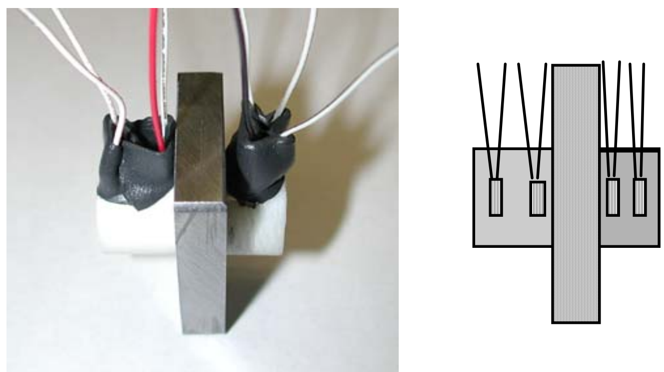

(a) (b)

Figure 1. (a) Constrained sample prior to testing and (b) schematic of setup.

Cylindrical samples, 15.7 mm in diameter, were core drilled from the plates in the through-thickness direction. Samples were compression tested over a wide range of displacement rates using the SHPB apparatus (the compression axis normal to fiber plane). However, the focus of the present report concerns a series of tests, all of which were conducted with striker bar velocities of 10, 16, or 20.5 m/s—as an approximate guide, these velocities would generate “average strain rates” of ~400, 500, and 700/s, respectively.

The particular SHPB apparatus used consists of Inconel[‡] 718 bars, a 356-mm-long striker bar, 3450-mm incident, and 1850-mm transmitter bars, all with a diameter of 19 mm. Further details of the experimental setup and standard data reduction routines are available elsewhere (*27*). Samples were fitted with strain gages, as shown in figure 1, so as to monitor real-time strains/stresses during the course of the tests. Strain gages with 0.79-mm element lengths were

[*]S-2 Glass is a registered trademark of Owens Corning.

[†]SC15 is a trademark of Applied Poleramic Incorporation..

[‡]Inconel is a registered trademark of the INCO family of companies.

used generally, although several tests were also carried out with an array of gages designed to sample the strain simultaneously at several locations along the sample length and thus provide a strain/time/position map of the wave passage.

A 3-D SHPB finite element model was used to study stress wave propagation in the multilayer materials and also in the individual components. Rubber is a highly nonlinear elastic material and the role of this nonlinear material has been studied by modeling the rubber layer with experimentally determined material data. The analyses were performed using a commercial explicit finite element code LS-DYNA 960. Two axes of symmetry were assumed, so only one quarter of the bar was modeled. For each test modeled, the output was displayed at several locations, within the sample as well as at the location of the strain gages on the incident and transmitter bars of the SHPB apparatus. The desired ideal result is that output from the strain gages on the incident and transmitter bars closely match data calculated from the model. Similarly, output measured by gages on the sample should also closely match data calculated from the model. When both these conditions are met, it indicates that the model is accurately capturing the wave propagation behavior in the sample and bars.

The model has four components in contact: a striker bar of 356 mm in length, an incident bar and a transmission bar each of 1524 mm in length, and the specimen, i.e., the ceramic, rubber, and composite layers, the thicknesses of which are 14, 1.5, and 10.6 mm, respectively. The bar diameter is 19.05 mm, and the diameter of the specimen is 16.0 mm. The component materials are modeled with 8-node solid elements, and the interfaces are modeled with the automatic contact sliding interfaces without friction. The impact velocity of the striker bar (V = 10, 16, and 20.5 m/s) has been defined as the initial condition, and all other boundaries are traction free and can move in any direction. In order to save computation time, the simulation uses bars 1524 mm in length, instead of full length bars. It will be seen later from the figures that this has the effect of decreasing the transit time between successive waves and shortening the wave duration slightly, however, it does not affect the basic wave shapes or amplitudes. A few trial computations were carried out using full-length bars, but apart from the slightly smaller time window, no significant differences were found, and the shorter bars were used henceforth.

Material properties used in the finite element code are shown in table 1. The ceramic was modeled with an isotropic elastic material model, and the composite was modeled with an orthotropic elastic material. Rubber was modeled with two different material models. The Mooney-Rivlin Model (*28*) (two parameter nonlinear material model) was used for the unconstrained configuration and the Blatz-Ko Material Model (*28*) was used for the constrained configuration. The Blatz-Ko Material Model shows better agreement for the hydrostatic state of stress of the rubber. For the unconstrained case, the rubber interlayer deforms very extensively, and this large deformation caused stability problems in the finite element model. This problem was solved by using different material parameters for the different cases. While higher shear modulus values give better results for the constrained case, in unconstrained samples, the lower shear modulus values give better agreement with the experimental results. Actual compression tests on the rubber itself confirm that this behavior is indeed observed in practice. To be able to use the same material model would probably be preferable, and this will be implemented for future simulations. The Inconel bars were modeled with an isotropic elastic material model, and lateral confinement of the rubber interlayer was modeled by preventing the displacements in both x and y directions for this component.

Table 1. Material properties used in finite element models.

Material	Modulus of Elasticity (GPa)	Poisson's Ratio	Density (kg/m^3)	Other
Ceramic	370	0.22	3900	—
Mooney-Rivlin rubber	—	0.495	1200	A:0.2 (MPa) B: 0.8 (MPa)
Blatz-Ko rubber	—	0.493	1200	G: 20 (MPa)
Composite	E_1: 40 E_2: 40 E_3: 15	ν_{21}: 0.12 ν_{31}: 0.173 ν_{32}: 0.173	1668	G_1: 8 (GPa) G_2: 8 (GPa) G_3: 8 (GPa)
Inconel	207	0.3	7850	—

3. Results

The experimental results are presented here in order of increasing incident bar velocity which corresponds to increasing loading rate and, as will become clear, increasing degrees of damage within the samples. Three different striker bar velocities were used, and SHPB tests and simulations were performed for both the unconstrained and the constrained situations. The primary data for each test consist of (1) experimental output from the SHPB bars for constrained and unconstrained specimens, (2) measured strain gage data from each sample, and (3) numerical data, which are then compared with the corresponding experiments.

3.1 Impact Velocity (10 m/s)

Figure 2 shows experimental and calculated SHPB data from an unconstrained sample tested at a striker bar velocity of 10 m/s, and close agreement is noted between the experimental and numerical results. Experimentally, it is seen that the transmitted wave amplitude slowly increases to ~60 MPa as indicated and exhibits a minor peak of ~100 μs before that. Calculated data show almost identical behavior.

Experimental data from the ceramic portion of an unconstrained strain-gaged sample are shown in figure 3a, while figure 3b shows the corresponding numerical data. The insets in the figure indicate the location of the gages or nodes interrogated. First, it is noted that the stress varies greatly with time and, second, it is noted that the stress close to the incident bar/ceramic interface

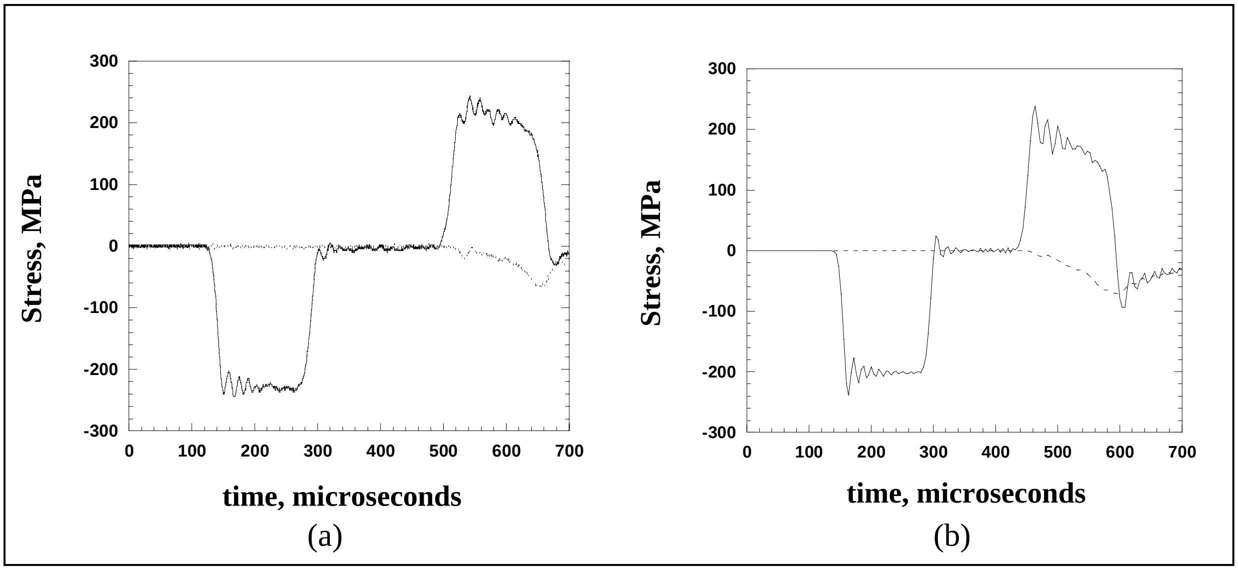

Figure 2. Stress on the incident and transmitter bars during a test at 10 m/s (unconstrained-rubber): (a) experimental and (b) calculated.

is invariably greater than that closer to the ceramic/rubber interface. Similarly, figure 3c and d shows experimental and calculated stresses measured on the composite portion of the sample.

Note that the magnitude of the initial peak in the composite layer is less than that in the ceramic layer and, again, an inhomogeneous stress distribution exists. Also, fewer large stress oscillations are noted than in the case of the ceramic. Generally, the numerical data show broadly similar behavior to the experimental data in each case, including multiple peaks in the ceramic, similar scale of stress inhomogeneity, similar magnitudes of the maximum stress, and a similar overall shape to each stress vs. time curve.

Figure 4 shows experimental and numerical SHPB data from a sample, tested at a striker bar velocity of 10 m/s, in which the rubber interlayer was constrained. Comparison with corresponding unconstrained data (figure 2a and b) shows that constraint greatly modifies the reflected and transmitted wave shapes. The constrained sample exhibits a maximum transmitted wave amplitude of ~200 MPa as compared to ~60 MPa for the unconstrained case. Figure 5 shows experimental and calculated stresses within the ceramic and composite, as a function of time, at different locations within the sample. It shows significantly different behavior compared to the unconstrained data, namely, what is essentially a single peak in the ceramic and composite and a more rapidly rising stress in both of the components when the rubber interlayer is constrained. The peak stress values in each component are almost the same value, i.e., ~250 MPa—considerably higher than when the rubber is unconstrained.

3.2 Impact Velocity (16 m/s)

When tested at an intermediate velocity, samples began to suffer limited damage, although none failed catastrophically. Lateral constraint of the rubber interlayer was found to increase the

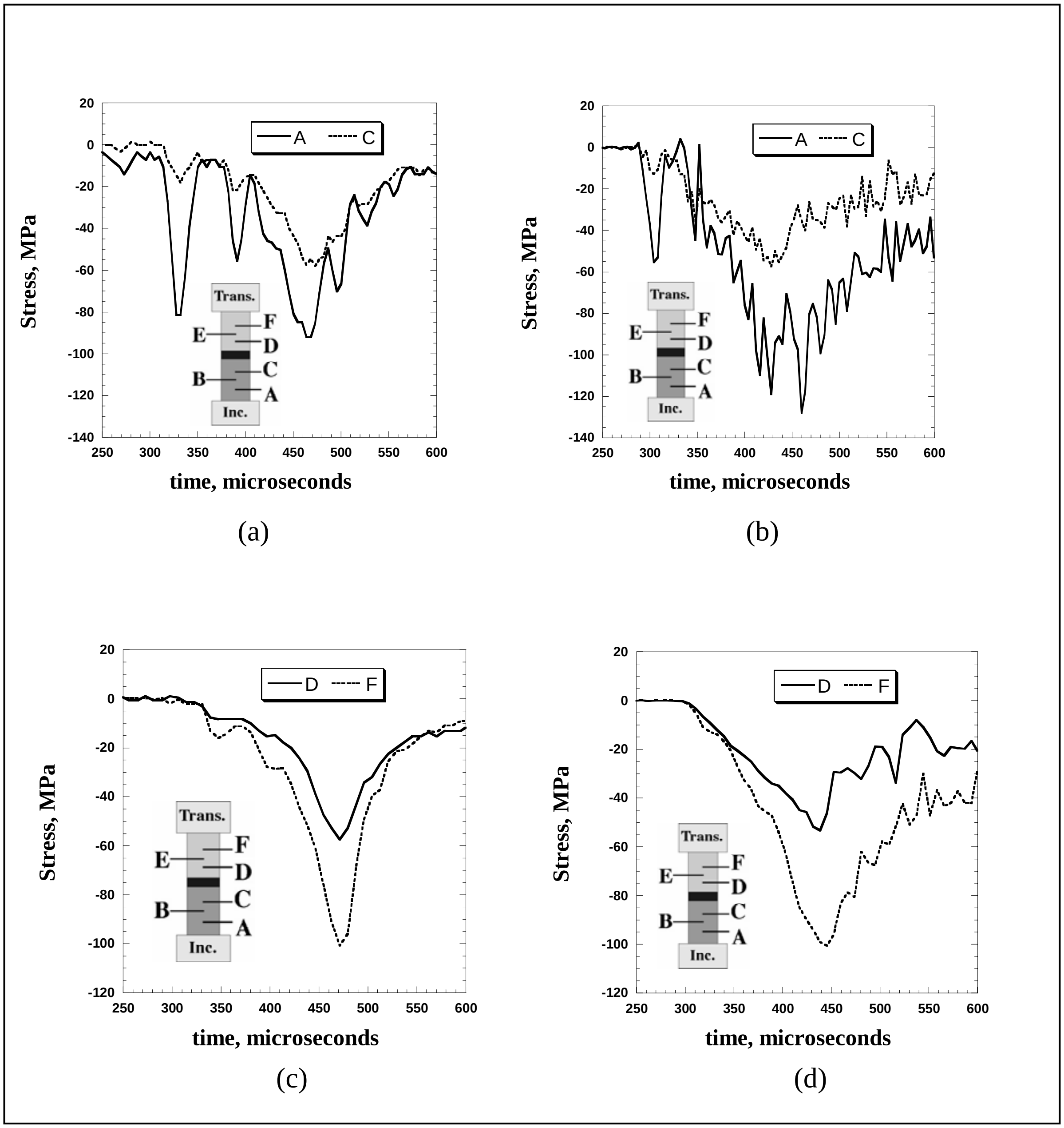

Figure 3. (a) Experimental and (b) calculated stress on ceramic: (c) experimental and (d) calculated stress on composite (unconstrained-rubber, V = 10 m/s).

damage level in both of the components. Visual damage in the composite exhibited itself as lateral spreading of the layers accompanied by significant radial strain, whereas the ceramic only exhibited occasional and limited spalling from the edges of the impacted face.

Figure 6a and b shows experimental SHPB data for the trilayer ceramic/rubber/composite with the rubber layer unconstrained and constrained, respectively. It is clear that the shapes of the transmitted and reflected waves for the constrained configuration are drastically different from the unconstrained case.

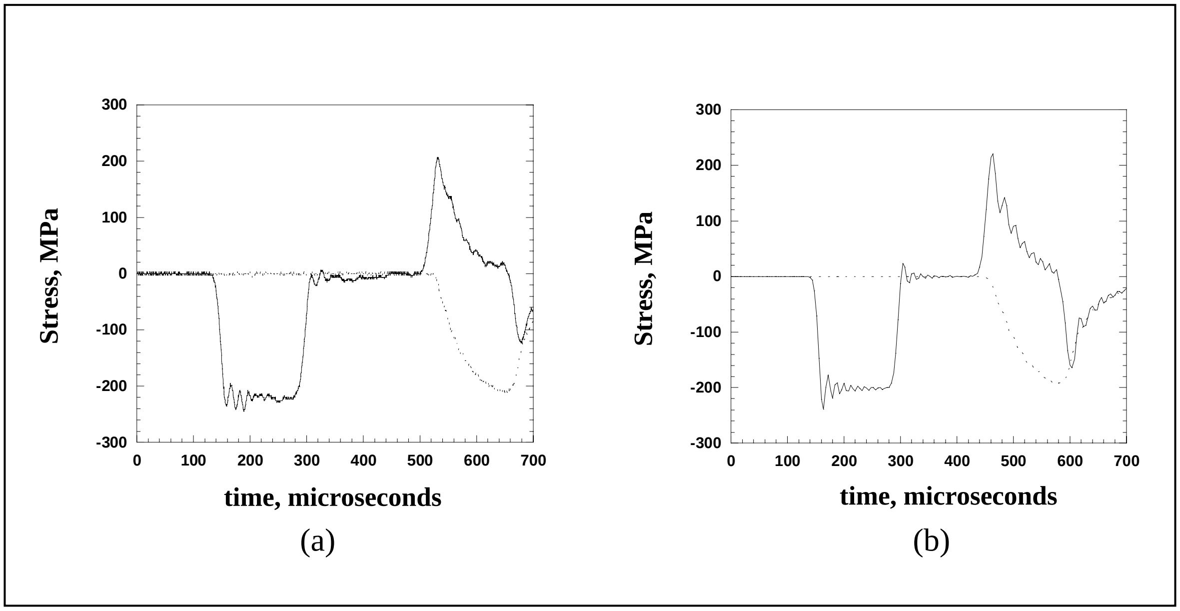

Figure 4. Stress on the incident and transmitter bars during a test at 10 m/s (constrained-rubber): (a) experimental and (b) calculated.

Major differences in the wave propagation characteristics, caused by lateral confinement of the rubber interlayer, are also clearly demonstrated in strain gage data collected from the separate layers. Figure 7a and b shows experimental data from the ceramic and composite layers, respectively. Data from gages on the ceramic show a marked increase in the measured stress levels resulting from confinement (figure 7a). Nevertheless, the general complexity of the wave forms of the unconstrained sample remains reminiscent of those tested at lower velocity (see figure 3a) insofar as three peaks may be discerned at ~65-µs intervals. The peaks present in the unconstrained case merge into essentially one peak when the rubber is constrained. In the composite, the maximum stress level experienced with constraint of the rubber interlayer is ~2.5× that for the unconstrained sample (figure 7b), while the corresponding stress in the ceramic increases by a factor of ~3.3.

Figure 8a and b shows the calculated data from the Hopkinson bars. For these samples, agreement between the experimental (figure 6a and b) and numerical data is currently slightly less close than for the low-velocity case, principally because damage has begun to occur in the experimental samples, but damage mechanisms have not yet been included in the present model, although they have been discussed elsewhere (*29*). The effect of damage initiation is reflected in a truncation of the early peak in the measured reflected wave.

Figure 9a and b shows numerical data from the individual ceramic and composite layers for the constrained and unconstrained cases. The elements chosen for the numerical data were at approximately the same position as the strain gages reported in figure 7. Comparison of these two figures shows that the calculated stress magnitudes are very similar to the experimental

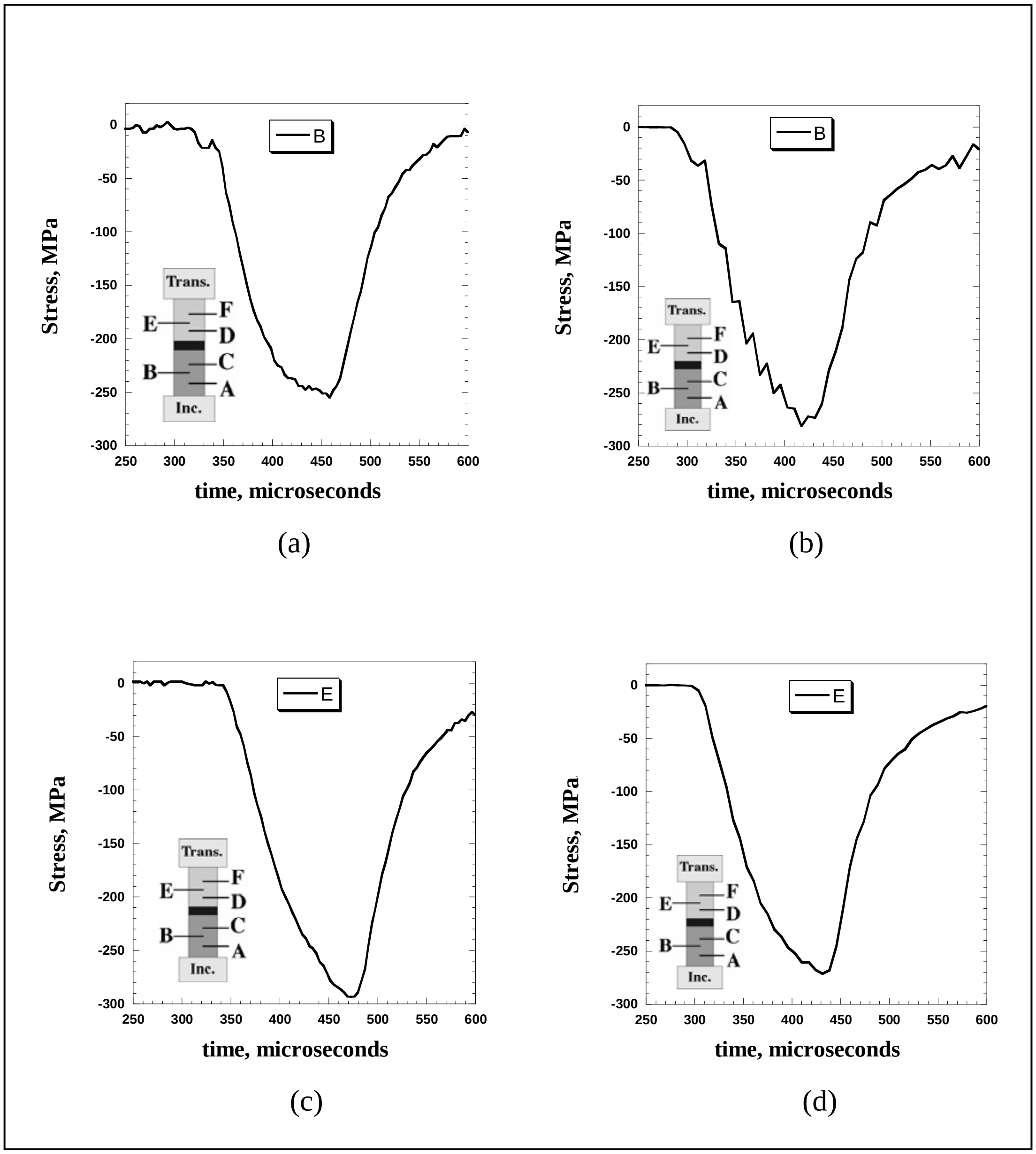

Figure 5. Stress on the specimen (constrained-rubber) tested at 10 m/s: (a) experimental and (b) calculated stress on ceramic: (c) experimental and (d) calculated stress on composite.

values. They differ only very slightly in detail as a result of the slight "stress-averaging" effect due to the finite size of the gages and, despite this, the same general shapes are found.

3.3 Impact Velocity (20.5 m/s)

A similar set of experiments and simulations was then carried out for a higher striker bar velocity. Now the presence of the rubber interlayer and its constraint leads to major differences in the wave propagation characteristics. Figure 10a and b shows experimental and calculated data from the incident and transmitter bars for the unconstrained rubber case. For this configuration, the basic shapes and magnitudes of the transmitted waves resemble each other, but

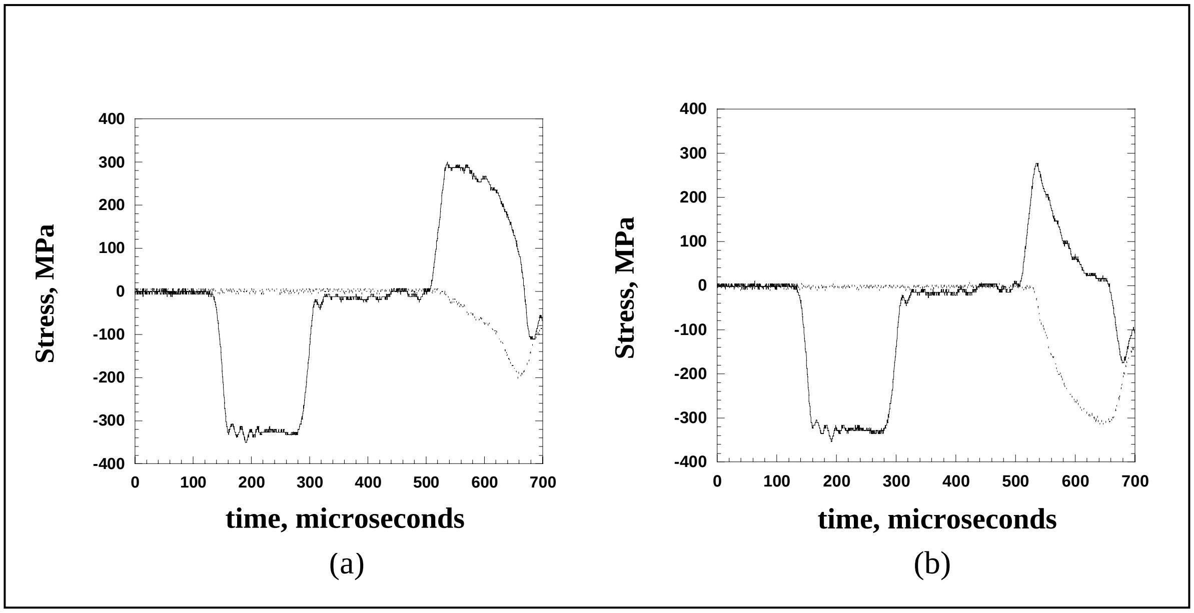

Figure 6. Stress measured on the incident and transmitter bars during a test at 16 m/s: (a) unconstrained rubber and (b) constrained rubber.

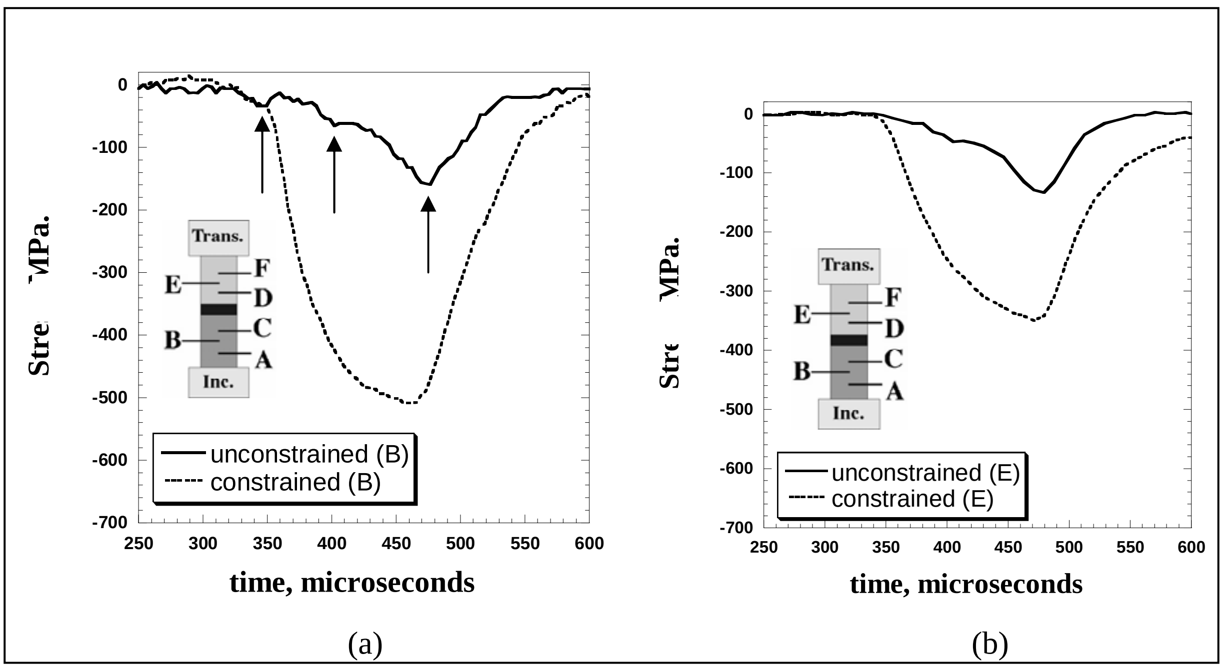

Figure 7. Experimental data from ceramic/rubber/composite tested at 16 m/s. Stress measured on (a) ceramic and (b) composite.

it is evident that significant physical damage begins to occur during the test at a stress of ~400 MPa, most clearly indicated by a change in the reflected wave shape.

Figure 11 shows experimental and numerical data from the individual ceramic and composite layers, respectively, with an unconstrained rubber interlayer. Figure 11a and c shows the actual

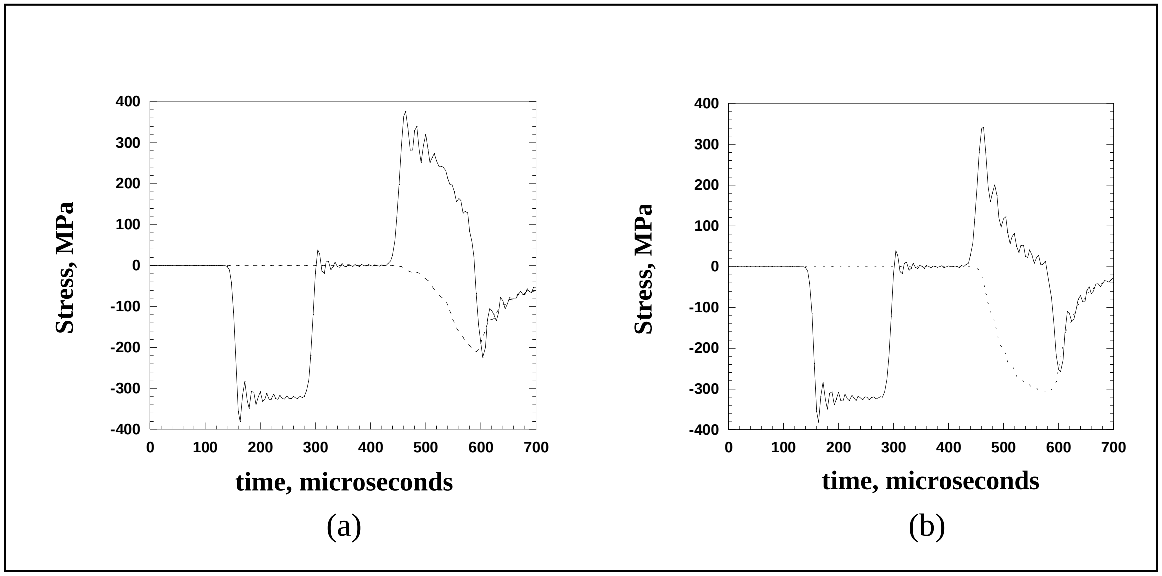

Figure 8. Calculated output from strain gages on the incident and transmitter bars during a test at 16 m/s: (a) unconstrained rubber and (b) constrained rubber.

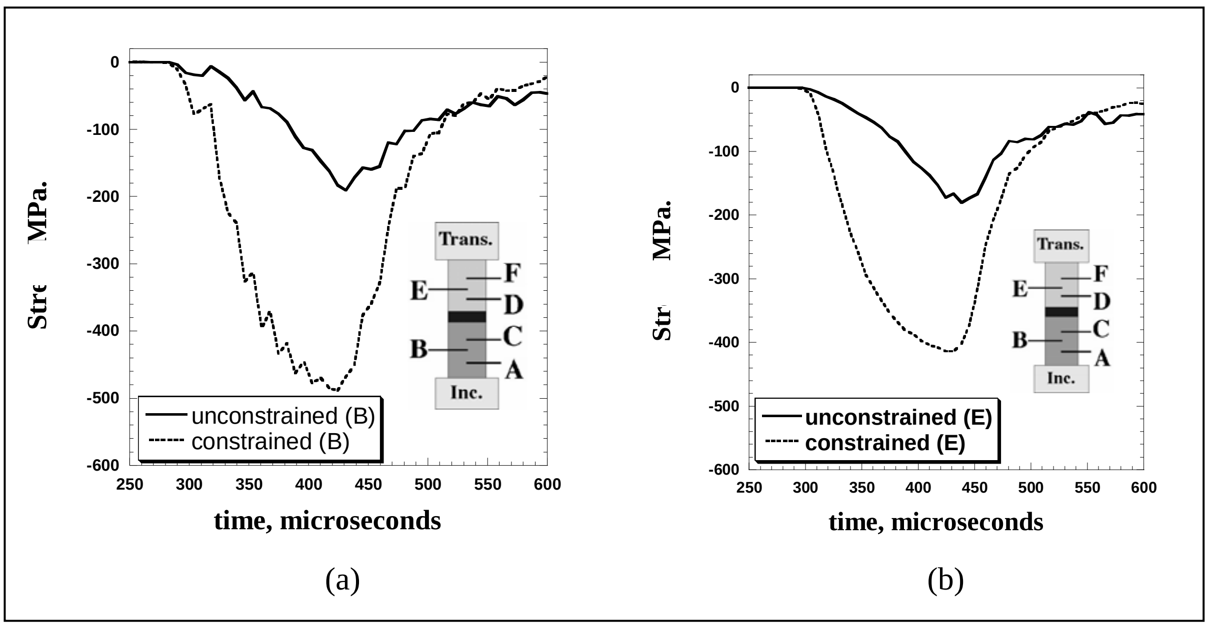

Figure 9. Calculated data from ceramic/rubber/composite (V = 16 m/s). Stress measured on (a) ceramic and (b) composite.

stress measured from two strain gages close to incident bar and rubber interfaces of the sample for the ceramic and, similarly, for the composite. (During this particular experiment, the gage close to the transmitter bar interface on the composite broke off due to the high strain at this location. As a result, only the initial portion of the stress read-out can be recorded for this gage.) Figure 11b shows the z-stress in the ceramic layer, calculated at two elements, at almost the same

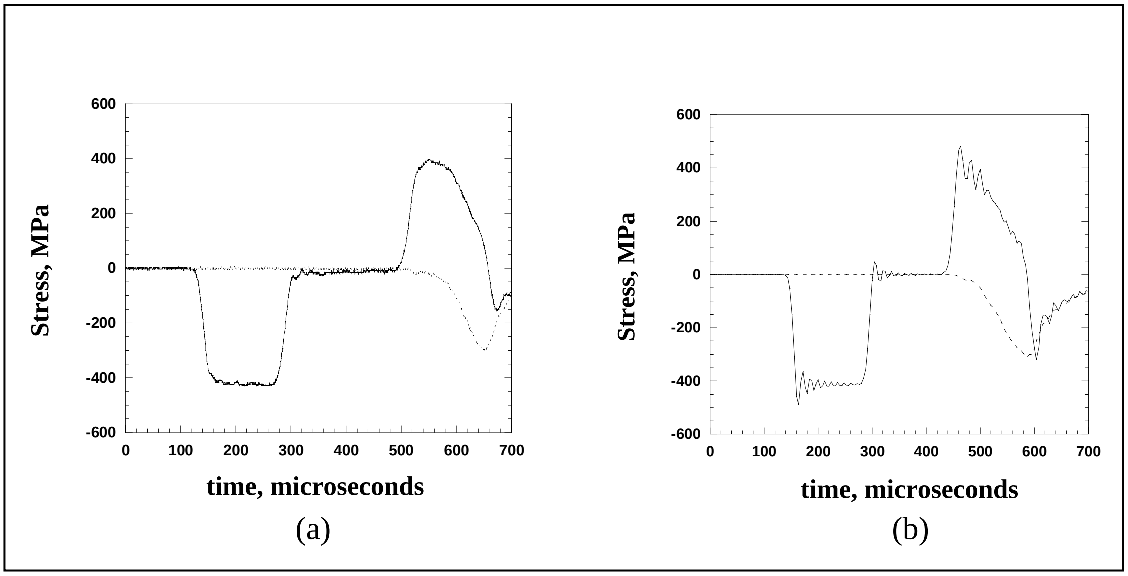

Figure 10. Stress on the incident and transmitter bars during a test at 20.5 m/s on an unconstrained ceramic/rubber/composite: (a) experimental and (b) calculated.

location as the experimental case. It can be clearly seen that during the course of testing the material experiences a nonuniform stress distribution, with the minimum occurring close to the rubber interlayer. Figure 11d shows calculated data from a similar element on the composite layer. Despite possible limitations of the present model due to damage initiation, it is seen that the calculated maximum stress levels are still very close to the measured stresses.

Figure 12a and b shows measured and calculated data from the incident and transmitter bars for the constrained rubber case. For these samples, agreement between the experimental and numerical data is again less close than for the unconstrained case at lower striker bar velocities (figures 6b and 8b) and the peak value of the reflected pulse has again been somewhat overestimated.

Figure 13 presents experimental and numerical data from the individual ceramic and composite layers. Figure 13a and c shows the actual stress measured from a single strain gage at midlength of the sample for the ceramic and composite. Similarly, figure 13b and d shows numerical data from the individual ceramic and composite layers at comparable locations. Comparison with figure 11 shows that a major effect of constraint is to broaden the principal peaks, resulting in the components remaining longer at these higher stress levels. The maximum stress is still experienced in each case (~140 μs) after the initial impact. Even for this high-impact velocity, the model still captures the general features of wave propagation and the form of stress distribution. The agreement in terms of absolute values of stress can also be clearly seen from the figures.

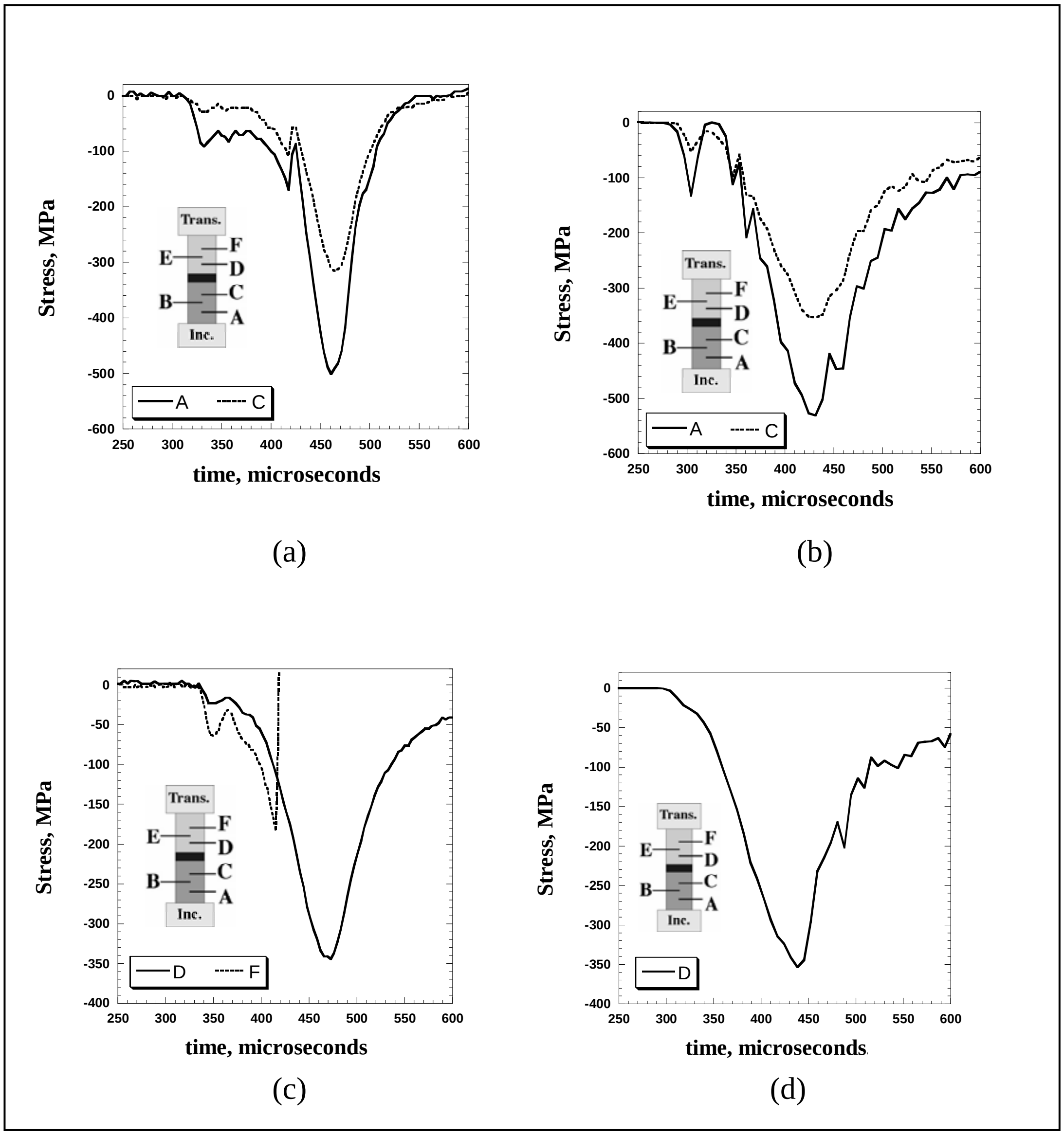

Figure 11. Stress measured on ceramic: (a) experimental and (b) calculated. Stress measured on composite: (c) experimental and (d) calculated (unconstrained-rubber, V = 20.5 m/s).

4. Discussion

The main objective of the present work was to investigate experimentally and numerically the effects of lateral confinement of the rubber interlayer on the wave propagation characteristics of the multilayer material over a range of impact velocities. The SHPB is a convenient tool for high strain rate testing of homogeneous elastic/plastic materials, but direct interpretation of SHPB data is not possible for materials which are nonlinear or of very low or very high

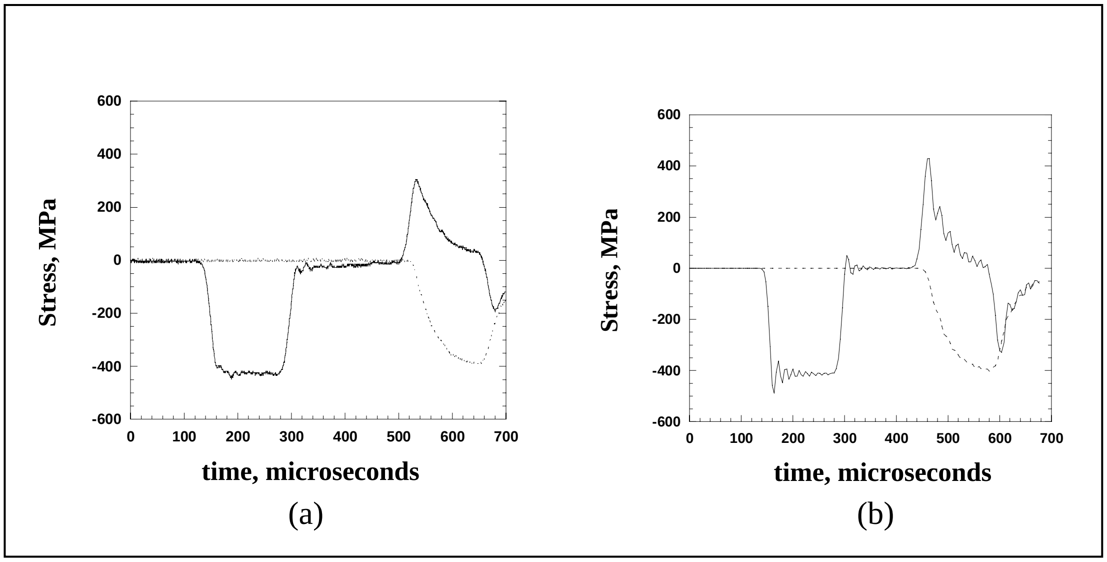

Figure 12. Stress measured on the incident and transmitter bars during a test at 20.5 m/s on a constrained ceramic/rubber/composite: (a) experimental and (b) calculated.

impedance relative to the bars, or anisotropic, or composed of several layers of distinctly different materials as in the case studied here. However, if numerical simulation procedures can be developed which satisfactorily reproduce the output data of SHPB tests, then (a) the tests themselves can be better interpreted and (b) simulations can be carried out with increased confidence.

A previous study (*25*) showed that there was excellent agreement between numerical data and actual data measured from the incident and transmitter bars for a two-layer ceramic/composite test. That model satisfactorily captured the details of wave transmission. The present three-layer model also satisfactorily captures the details of wave transmission, the general features of wave propagation, stress magnitudes, and the form of stress distribution, and consequently offers considerably enhanced insight into the processes leading to damage generation in such multilayer materials.

The experiments are subject to some limitation because the strain gages average the data over their active gage length, which is typically 0.79 mm as compared with ~0.4 mm for the element size in the model. Also, the measured stress is seen to be very strongly dependent upon the exact placement of the gage within the specimen length. Finally, some of the strain gages mounted on the components could not record all the stress wave history either because of their failure or because of the high strain levels generated in the components (see figure 11c).

Keeping these limitations in mind, it can be appreciated that there is nonetheless good agreement between experimental and numerical data even for the highest impact velocity tests. For example, figure 3a shows experimental data from two gages (5 mm apart) on the ceramic sample

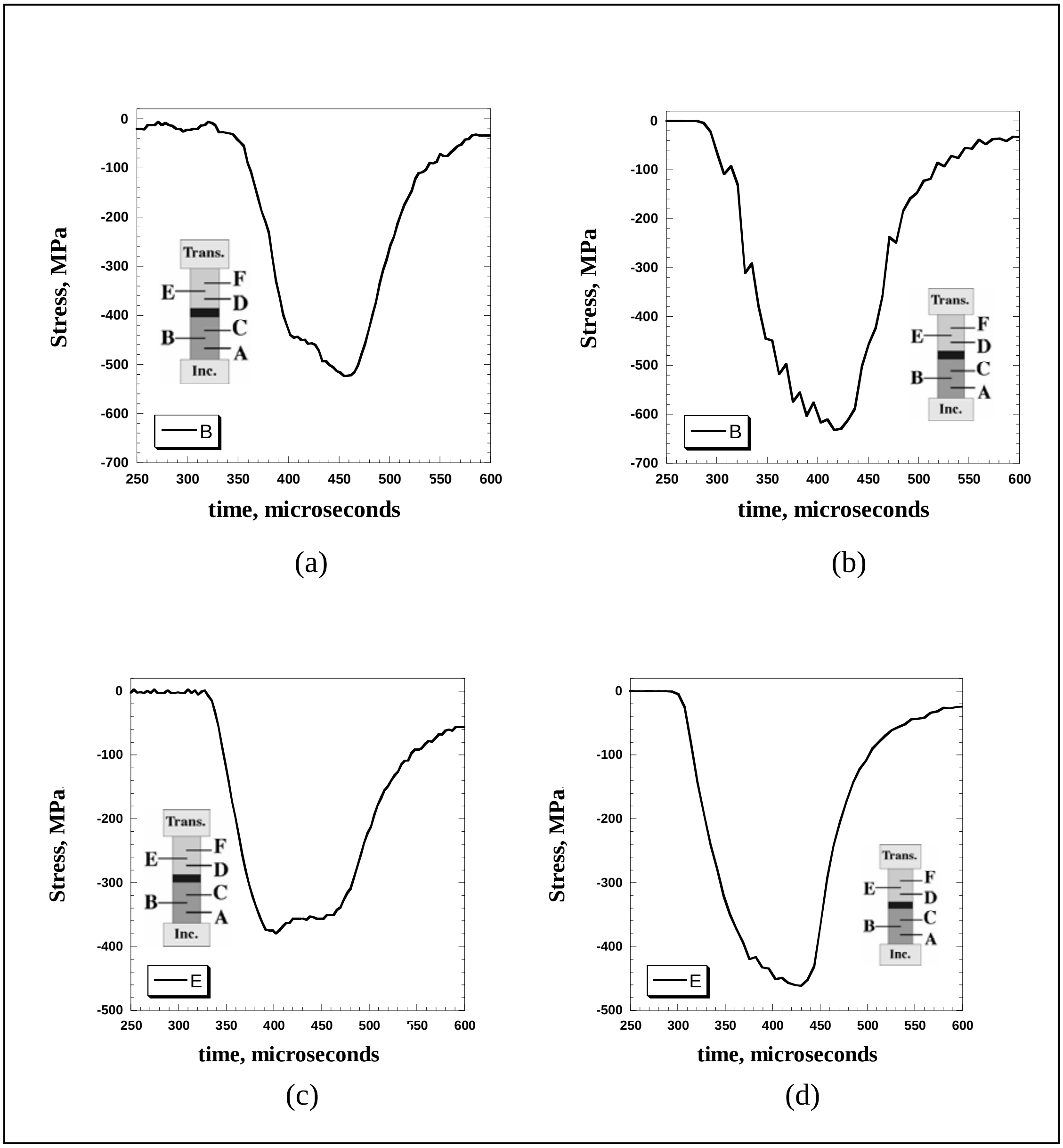

Figure 13. Stress measured on ceramic: (a) experimental and (b) calculated: Stress measured on composite: (c) experimental and (d) calculated (constrained-rubber, V = 20.5 m/s).

surface. After the initial stress peak, a second major peak is observed ~150 μs later; the numerical data (figure 3b) likewise show the initial and second peak stresses at approximately similar intervals. Furthermore, interpolating to comparable elemental positions, the relative magnitudes are quite similar. The absolute magnitudes of the maximum measured stresses are, however, slightly different, and this is partially due to reasons of data source location and the "averaging" effect of the strain gage size previously mentioned.

Throughout all the current sets of experiments and simulations, close agreement was achieved between the model and experiment. Figures 6a and b and 8a and b show experimental and calculated data from the Hopkinson bars. Again, the data match closely, showing that LS-DYNA accurately captures the details of wave propagation.

A major conclusion from the present results is that constraint of the rubber layer drastically alters the response of the material, and this is most easily demonstrated by the change of the reflected and transmitted wave shapes. For example, in the case of the lowest velocity tests, instead of reaching a maximum transmitted stress of ~60 MPa, as for the unconstrained case, the maximum stress is ~210 MPa when constrained (compare figures 2a and 4a). Also the stress rises relatively faster and more uniformly for the second case: basically, lateral confinement of the rubber interlayer increases the wave transmission efficiency between the components.

It can also be seen that the shapes of the wave traveling through the individual ceramic and composite layers are widely different in the unconstrained material, an observation that is confirmed both by experimental measurements and numerical analysis. For example, figure 3 shows that an almost instantaneous and rapid stress increase occurs for the ceramic, followed by further major oscillations, while the composite shows a largely monotonic and gradual increase in stress level. By contrast, in constrained samples, the wave shapes are almost the same for the ceramic and composite (see figure 5) and come to resemble the shape of the wave traveling in the composite. In other words and in common with many other kinetic processes, the component of lowest impedance dominates the process.

Rubber leads to a highly inhomogeneous stress distribution within the components when it is constrained. Generally, the part of the sample close to the unconstrained rubber experiences a reduced stress while the remainder may experience a much higher stress level. However, when the rubber is constrained, the differences in stress level within the components are greatly reduced, although the stress is still by no means homogeneous.

For the higher velocity tests, agreement between the experimental and numerical data is currently slightly less close than for the lower velocity cases (see figures 10–13), for reasons associated with damage evolution. During testing at high velocities, the ceramic frequently shattered, and various damage modes were activated in the composite. Even though the material models used in this study do not include failure parameters, the numerical calculations still capture the general features of wave propagation and the form of stress distribution. Obviously, further refinement along these lines will significantly improve agreement between experiment and model.

In this respect, the present work indicates several avenues for characterizing damage evolution in these, or similar materials at high strain rates since the effects of damage are clearly indicated in the output signals. For example, the principal differences between figures 4a and 10a can be ascribed to the onset of significant damage that alters the (here assumed elastic) properties of the materials. Therefore, the point at which experimental and numerical data begin to diverge probably defines the point at which significant damage begins. It is thus possible to study, by comparison of experimental and numerical data, damage evolution at high strain rate indirectly as a function of strain and strain rate. When coupled with microscopic examination of recovered material, the present type of data would elucidate the processes and sequence of deformation and fracture events.

This is potentially of great utility because failure criteria are included in recent material models, but a definition of stress and strain levels associated with these events is presently rather imprecise. So, if stress or strain levels associated with the onset of various damage mechanisms can be determined, these could be inserted into the numerical models and provide improved accuracy.

5. Conclusions

The present work has demonstrated the feasibility of modeling stress wave propagation in complex multilayer materials. It has been shown that the effects of confinement of normally low modulus materials can significantly affect their response to wave propagation. Severe stress inhomogeneities and discontinuities may exist in multilayer materials, and these may have serious consequences for the mechanical and other properties. Numerical modeling clearly shows that during Hopkinson bar testing of multilayer materials, stress is not distributed uniformly inside the specimen. The one-dimensional stress state usually assumed for conventional SHPB testing is questionable, and for a complete understanding of the wave propagation, both numerical and experimental results have to be coupled. In this study, both methods were used, and the stress states inside the components were presented. Accuracy will be increased, especially for the high pressure levels, by implementing damage parameters in future material models.

6. References

1. Lee, S.; Sun, C. Dynamic Penetration of Graphite-Epoxy Laminates Impacted by a Blunt-Ended Projectile. *Composites Science and Technology* **1993**, *49* (4), 369–380.

2. Goldsmith, W.; Dharan, C.; Chang, H. Quasi-Static and Ballistic Perforation of Carbon-Fiber Laminates. *International Journal of Solids and Structures* **1995**, *32* (1), 89–103.

3. Wu, E.; Chang, L. Loading Rate Effect on Woven Glass Laminated Plates by Penetration Force. *Journal of Composite Materials* **1998**, *32* (8), 702–721.

4. Abrate, S. Modeling of Impact on Composite Structures. *Comp. Struct.* **2001**, *51*, 129–138.

5. Collombet, F.; Lalbin, X.; Bonini, J.; Martin, V.; Lataillade, J. L. Damage Criteria for the Study of Impacted Composite Laminates. *Composites Science and Technology* **1998**, *58* (5), 679–686.

6. Chen, W.; Ravichandran, G. Dynamic Compressive Failure of a Glass Ceramic Under Lateral Confinement. *Journal of the Mechanics and Physics of Solids* **1997**, *45* (8), 1303–1328.

7. DeLuca, E.; Prifti, J.; Betheney, W.; Chou, S. C. Ballistic Impact Damage of S-2 Glass-Reinforced Plastic Structural Armor. *Composites Science and Technology* **1998**, *58* (9), 1453–1461.

8. Gama, B. A.; Gillespie, J. W., Jr.; Mahfuz, H.; Raines, R. P.; Haque, A.; Jeelani, S.; Bogetti, T. A.; Fink, B. K. High Strain-Rate Behavior of Plain-Weave S-2 Glass/Vinyl Ester Composites. *Journal of Composite Materials* **2001**, *35* (13), 1201–1228.

9. Kim, J.; Kang, K. An Analysis of Impact Force in Plain-Weave Glass/Epoxy Composite Plates Subjected to Transverse Impact. *Composites Science and Technology* **2001**, *61* (1), 135–143.

10. Cantwell, W.; Morton, J. Geometrical Effects in the Low Velocity Impact Response of Cfrp. *Composite Structures* **1989**, *12* (1), 39–59.

11. Mines, R.; Roach, A.; Jones, N. High Velocity Perforation Behaviour of Polymer Composite Laminates. *International Journal of Impact Engineering* **1999**, *22* (6), 561–588.

12. Wen, H. Penetration and Perforation of Thick FRP Laminates. *Composites Science and Technology* **2001**, *61* (8), 1163–1172.

13. Li, Y.; Ramesh, K.; Chin, E. Dynamic Characterization of Layered and Graded Structures Under Impulsive Loading. *International Journal of Solids and Structures* **2001**, *38* (34, 35), 6045–6061.

14. Fink, B. Performance Metrics for Composite Integral Armor. *Journal of Thermoplastic Composite Materials* **2000**, *13* (5), 417–431.

15. Gama, B.; Bogetti, T. A.; Fink, B. K.; Yu, C. J.; Claar, T. D.; Eifert, H. H.; Gillespie, J. W., Jr. Aluminum Foam Integral Armor: A New Dimension in Armor Design. *Composite Structures* **2001**, *52* (3, 4), 381–395.

16. Gama, B.; Gillespie, J. W., Jr.; Bogetti, T.; Fink, B. Innovative Design and Ballistic Performance of Lightweight Composite Integral Armor. In *SAE 2001 World Congress*; SAE: Detroit, MI, 2001.

17. Gama, B.; Gillespie, J. W., Jr.; Mahfuz, H.; Bogetti, T.; Fink, B. Effect of Non-Linear Material Behavior on the Through-Thickness Stress Wave Propagation in Multi-Layer Hybrid Lightweight Armor. In *Advances in Comp. Eng. and Sci.*; Tech. Sci. Press: Palmdale, CA, 2000; Vol. I, pp. 157–162.

18. Mahfuz, H.; Zhu, Y. H.; Haque, A.; Abutalib, A.; Vaidya, U.; Jeelani, S.; Gama, B. A.; Gillespie, J. W., Jr. Investigation of High-Velocity Impact on Integral Armor Using Finite Element Method. *International Journal of Impact Engineering* **2000**, *24* (2), 203–217.

19. Jovicic, J.; Zavaliangos, A.; Ko, F. Modeling of the Ballistic Behavior of Gradient Design Composite Armors. *Composites Part A - Applied Science and Manufacturing* **2000**, *31* (8), 773–784.

20. Martinez, M. A.; Chocron, I. S.; Rodriguez, J.; Galvez, V. S.; Sastre, L. A. Confined Compression of Elastic Adhesives at High Rates of Strain. *International Journal of Adhesion and Adhesives* **1998**, *18* (6), 375–383.

21. Gupta, Y.; Ding, J. Impact Load Spreading in Layered Materials and Structures: Concept and Quantitative Measure. *International Journal of Impact Engineering* **2002**, *27* (3), 277–291.

22. Verleysen, P.; Degrieck, J. Improved Signal Processing for Split Hopkinson Bar Tests on (Quasi-)Brittle Materials. *Experimental Techniques* **2000**, *24* (6), 31–33.

23. Bacon, C. Separation of Waves Propagating in an Elastic or Viscoelastic Hopkinson Pressure Bar With Three-Dimensional Effects. *International Journal of Impact Engineering* **1999**, *22* (1), 55–69.

24. Gama, B.; Lopatnikov, S.; Gillespie, J. W., Jr. Numerical Hopkinson Bar Analysis: Validity of One-Dimensional Assumptions. *CD Proceedings, ASC 2003 Conference*, Gainesville, FL, 20–22 October 2003.

25. Tasdemirci, A.; Hall, I.; Gama, B.; Guden, M. Stress Wave Propagation Effects in Multi-Component Composite Materials. *Journal of Composite Materials* **2003**, *38* (12), 995–1011.

26. Espinosa, H. D.; Brar, N. S.; Yuan, G.; Xu, Y.; Arrieta, V. Enhanced Ballistic Performance of Confined Multi-Layered Ceramic Targets Against Long Rod Penetrators Through Interface Defeat. *International Journal of Solids and Structures* **2000**, *37* (36), 4893–4913.

27. Guden, M.; Hall, I. Dynamic Properties of Metal Matrix Composites: A Comparative Study. *Materials Science and Engineering A-Structural Materials Properties Microstructure and Processing* **1998**, *242* (1, 2), 141–152.

28. *LS-DYNA Keyword User's Manual Version 970*; Livermore Software Technology (LSTC) Corporation: Livermore, CA, 2003.

29. Yen, C. F. Ballistic Impact Modeling of Composite Materials. In *7th International LS-DYNA Users Conference*, Dearborn, MI, 2002; LSTC and Engineering Technology Associates, Inc. (ETA).

NO. OF COPIES	ORGANIZATION
1	DEFENSE TECHNICAL
1 (PDF ONLY)	DEFENSE TECHNICAL INFORMATION CTR DTIC OCA 8725 JOHN J KINGMAN RD STE 0944 FT BELVOIR VA 22060-6218
1	COMMANDING GENERAL US ARMY MATERIEL CMD AMCRDA TF 5001 EISENHOWER AVE ALEXANDRIA VA 22333-0001
1	INST FOR ADVNCD TCHNLGY THE UNIV OF TEXAS AT AUSTIN 3925 W BRAKER LN STE 400 AUSTIN TX 78759-5316
1	US MILITARY ACADEMY MATH SCI CTR EXCELLENCE MADN MATH THAYER HALL WEST POINT NY 10996-1786
1	DIRECTOR US ARMY RESEARCH LAB IMNE AD IM DR 2800 POWDER MILL RD ADELPHI MD 20783-1197
3	DIRECTOR US ARMY RESEARCH LAB AMSRD ARL CI OK TL 2800 POWDER MILL RD ADELPHI MD 20783-1197
3	DIRECTOR US ARMY RESEARCH LAB AMSRD ARL CS IS T 2800 POWDER MILL RD ADELPHI MD 20783-1197

NO. OF COPIES	ORGANIZATION
	ABERDEEN PROVING GROUND
1	DIR USARL AMSRD ARL CI OK TP (BLDG 4600)

NO. OF COPIES	ORGANIZATION
1	DIRECTOR US ARMY RESEARCH LAB AMSRD ARL SE L D SNIDER 2800 POWDER MILL RD ADELPHI MD 20783-1197
1	DIRECTOR US ARMY RESEARCH LAB AMSRD ARL SE DE R ATKINSON 2800 POWDER MILL RD ADELPHI MD 20783-1197
5	DIRECTOR US ARMY RESEARCH LAB AMSRD ARL WM MB A ABRAHAMIAN M BERMAN M CHOWDHURY T LI E SZYMANSKI 2800 POWDER MILL RD ADELPHI MD 20783-1197
1	COMMANDER US ARMY MATERIEL CMD AMXMI INT 5001 EISENHOWER AVE ALEXANDRIA VA 22333-0001
2	PM MAS SFAE AMO MAS MC PICATINNY ARSENAL NJ 07806-5000
3	COMMANDER US ARMY ARDEC AMSTA AR CC M PADGETT J HEDDERICH H OPAT PICATINNY ARSENAL NJ 07806-5000
2	COMMANDER US ARMY ARDEC AMSTA AR AE WW E BAKER J PEARSON PICATINNY ARSENAL NJ 07806-5000

NO. OF COPIES	ORGANIZATION
1	COMMANDER US ARMY ARDEC AMSTA AR FSE PICATINNY ARSENAL NJ 07806-5000
1	COMMANDER US ARMY ARDEC AMSTA AR TD PICATINNY ARSENAL NJ 07806-5000
13	COMMANDER US ARMY ARDEC AMSTA AR CCH A F ALTAMURA M NICOLICH M PALATHINGUL D VO R HOWELL A VELLA M YOUNG L MANOLE S MUSALLI R CARR M LUCIANO E LOGSDEN T LOUZEIRO PICATINNY ARSENAL NJ 07806-5000
1	COMMANDER US ARMY ARDEC AMSTA AR CCH P J LUTZ PICATINNY ARSENAL NJ 07806-5000
1	COMMANDER US ARMY ARDEC AMSTA AR FSF T C LIVECCHIA PICATINNY ARSENAL NJ 07806-5000
1	COMMANDER US ARMY ARDEC AMSTA ASF PICATINNY ARSENAL NJ 07806-5000

NO. OF COPIES	ORGANIZATION
1	COMMANDER US ARMY ARDEC AMSTA AR QAC T C J PAGE PICATINNY ARSENAL NJ 07806-5000
1	COMMANDER US ARMY ARDEC AMSTA AR M D DEMELLA PICATINNY ARSENAL NJ 07806-5000
3	COMMANDER US ARMY ARDEC AMSTA AR FSA A WARNASH B MACHAK M CHIEFA PICATINNY ARSENAL NJ 07806-5000
2	COMMANDER US ARMY ARDEC AMSTA AR FSP G M SCHIKSNIS D CARLUCCI PICATINNY ARSENAL NJ 07806-5000
2	COMMANDER US ARMY ARDEC AMSTA AR CCH C H CHANIN S CHICO PICATINNY ARSENAL NJ 07806-5000
1	COMMANDER US ARMY ARDEC AMSTA AR QAC T D RIGOGLIOSO PICATINNY ARSENAL NJ 07806-5000
1	COMMANDER US ARMY ARDEC AMSTA AR WET T SACHAR BLDG 172 PICATINNY ARSENAL NJ 07806-5000
1	US ARMY ARDEC INTELLIGENCE SPECIALIST AMSTA AR WEL F M GUERRIERE PICATINNY ARSENAL NJ 07806-5000
10	COMMANDER US ARMY ARDEC AMSTA AR CCH B P DONADIA F DONLON P VALENTI C KNUTSON G EUSTICE K HENRY J MCNABOC G WAGNECZ R SAYER F CHANG PICATINNY ARSENAL NJ 07806-5000
6	COMMANDER US ARMY ARDEC AMSTA AR CCL F PUZYCKI R MCHUGH D CONWAY E JAROSZEWSKI R SCHLENNER M CLUNE PICATINNY ARSENAL NJ 07806-5000
1	PM ARMS SFAE GCSS ARMS BLDG 171 PICATINNY ARSENAL NJ 07806-5000
1	COMMANDER US ARMY ARDEC AMSTA AR WEA J BRESCIA PICATINNY ARSENAL NJ 07806-5000
1	PM MAS SFAE AMO MAS PICATINNY ARSENAL NJ 07806-5000

NO. OF COPIES	ORGANIZATION
1	PM MAS SFAE AMO MAS CHIEF ENGINEER PICATINNY ARSENAL NJ 07806-5000
1	PM MAS SFAE AMO MAS PS PICATINNY ARSENAL NJ 07806-5000
2	PM MAS SFAE AMO MAS LC PICATINNY ARSENAL NJ 07806-5000
1	COMMANDER US ARMY ARDEC PRODUCTION BASE MODERN ACTY AMSMC PBM K PICATINNY ARSENAL NJ 07806-5000
1	COMMANDER US ARMY TACOM PM COMBAT SYSTEMS SFAE GCS CS 6501 ELEVEN MILE RD WARREN MI 48397-5000
1	COMMANDER US ARMY TACOM AMSTA SF WARREN MI 48397-5000
1	DIRECTOR AIR FORCE RESEARCH LAB MLLMD D MIRACLE 2230 TENTH ST WRIGHT PATTERSON AFB OH 45433-7817
1	OFC OF NAVAL RESEARCH J CHRISTODOULOU ONR CODE 332 800 N QUINCY ST ARLINGTON VA 22217-5600
1	US ARMY CERL R LAMPO 2902 NEWMARK DR CHAMPAIGN IL 61822

NO. OF COPIES	ORGANIZATION
1	COMMANDER US ARMY TACOM PM SURVIVABLE SYSTEMS SFAE GCSS W GSI H M RYZYI 6501 ELEVEN MILE RD WARREN MI 48397-5000
1	COMMANDER US ARMY TACOM CHIEF ABRAMS TESTING SFAE GCSS W AB QT T KRASKIEWICZ 6501 ELEVEN MILE RD WARREN MI 48397-5000
1	COMMANDER WATERVLIET ARSENAL SMCWV QAE Q B VANINA BLDG 44 WATERVLIET NY 12189-4050
1	TNG, DOC, & CBT DEV ATZK TDD IRSA A POMEY FT KNOX KY 40121
2	HQ IOC TANK AMMUNITION TEAM AMSIO SMT R CRAWFORD W HARRIS ROCK ISLAND IL 61299-6000
2	COMMANDER US ARMY AMCOM AVIATION APPLIED TECH DIR J SCHUCK FT EUSTIS VA 23604-5577
1	NSWC DAHLGREN DIV CODE G06 DAHLGREN VA 22448
2	US ARMY CORPS OF ENGR CERD C T LIU CEW ET T TAN 20 MASSACHUSETTS AVE NW WASHINGTON DC 20314

NO. OF COPIES	ORGANIZATION
1	US ARMY COLD REGIONS RSCH & ENGRNG LAB P DUTTA 72 LYME RD HANOVER NH 03755
14	COMMANDER US ARMY TACOM AMSTA TR R R MCCLELLAND D THOMAS J BENNETT D HANSEN AMSTA JSK S GOODMAN J FLORENCE K IYER D TEMPLETON A SCHUMACHER AMSTA TR D D OSTBERG L HINOJOSA B RAJU AMSTA CS SF H HUTCHINSON F SCHWARZ WARREN MI 48397-5000
14	BENET LABS AMSTA AR CCB R FISCELLA M SOJA E KATHE M SCAVULO G SPENCER P WHEELER S KRUPSKI J VASILAKIS G FRIAR R HASENBEIN AMSTA CCB R S SOPOK E HYLAND D CRAYON R DILLON WATERVLIET NY 12189-4050
1	USA SBCCOM PM SOLDIER SPT AMSSB PM RSS A J CONNORS KANSAS ST NATICK MA 01760-5057

NO. OF COPIES	ORGANIZATION
1	NSWC TECH LIBRARY CODE 323 17320 DAHLGREN RD DAHLGREN VA 22448
2	USA SBCCOM MATERIAL SCIENCE TEAM AMSSB RSS J HERBERT M SENNETT KANSAS ST NATICK MA 01760-5057
2	OFC OF NAVAL RESEARCH D SIEGEL CODE 351 J KELLY 800 N QUINCY ST ARLINGTON VA 22217-5660
1	NSWC CRANE DIVISION M JOHNSON CODE 20H4 LOUISVILLE KY 40214-5245
2	NSWC U SORATHIA C WILLIAMS CD 6551 9500 MACARTHUR BLVD WEST BETHESDA MD 20817
2	COMMANDER NSWC CARDEROCK DIVISION R PETERSON CODE 2020 M CRITCHFIELD CODE 1730 BETHESDA MD 20084
8	DIRECTOR US ARMY NGIC D LEITER MS 404 M HOLTUS MS 301 M WOLFE MS 307 S MINGLEDORF MS 504 J GASTON MS 301 W GSTATTENBAUER MS 304 R WARNER MS 305 J CRIDER MS 306 2055 BOULDERS RD CHARLOTTESVILLE VA 22911-8318

NO. OF COPIES	ORGANIZATION
1	NAVAL SEA SYSTEMS CMD D LIESE 1333 ISAAC HULL AVE SE 1100 WASHINGTON DC 20376-1100
1	EXPEDITIONARY WARFARE DIV N85 F SHOUP 2000 NAVY PENTAGON WASHINGTON DC 20350-2000
8	US ARMY SBCCOM SOLDIER SYSTEMS CENTER BALLISTICS TEAM J WARD W ZUKAS P CUNNIFF J SONG MARINE CORPS TEAM J MACKIEWICZ BUS AREA ADVOCACY TEAM W HASKELL AMSSB RCP SS W NYKVIST S BEAUDOIN KANSAS ST NATICK MA 01760-5019
7	US ARMY RESEARCH OFC A CROWSON H EVERETT J PRATER G ANDERSON D STEPP D KISEROW J CHANG PO BOX 12211 RESEARCH TRIANGLE PARK NC 27709-2211
1	AFRL MLBC 2941 P ST RM 136 WRIGHT PATTERSON AFB OH 45433-7750
1	DIRECTOR LOS ALAMOS NATL LAB F L ADDESSIO T 3 MS 5000 PO BOX 1633 LOS ALAMOS NM 87545

NO. OF COPIES	ORGANIZATION
8	NSWC J FRANCIS CODE G30 D WILSON CODE G32 R D COOPER CODE G32 J FRAYSSE CODE G33 E ROWE CODE G33 T DURAN CODE G33 L DE SIMONE CODE G33 R HUBBARD CODE G33 DAHLGREN VA 22448
1	NSWC CARDEROCK DIVISION R CRANE CODE 6553 9500 MACARTHUR BLVD WEST BETHESDA MD 20817-5700
1	AFRL MLSS R THOMSON 2179 12TH ST RM 122 WRIGHT PATTERSON AFB OH 45433-7718
2	AFRL F ABRAMS J BROWN BLDG 653 2977 P ST STE 6 WRIGHT PATTERSON AFB OH 45433-7739
5	DIRECTOR LLNL R CHRISTENSEN S DETERESA F MAGNESS M FINGER MS 313 M MURPHY L 282 PO BOX 808 LIVERMORE CA 94550
1	AFRL MLS OL L COULTER 5851 F AVE BLDG 849 RM AD1A HILL AFB UT 84056-5713
1	OSD JOINT CCD TEST FORCE OSD JCCD R WILLIAMS 3909 HALLS FERRY RD VICKSBURG MS 29180-6199

NO. OF COPIES	ORGANIZATION
3	DARPA M VANFOSSEN S WAX L CHRISTODOULOU 3701 N FAIRFAX DR ARLINGTON VA 22203-1714
2	SERDP PROGRAM OFC PM P2 C PELLERIN B SMITH 901 N STUART ST STE 303 ARLINGTON VA 22203
1	OAK RIDGE NATL LAB R M DAVIS PO BOX 2008 OAK RIDGE TN 37831-6195
1	OAK RIDGE NATL LAB C EBERLE MS 8048 PO BOX 2008 OAK RIDGE TN 37831
3	DIRECTOR SANDIA NATL LABS APPLIED MECHS DEPT MS 9042 J HANDROCK Y R KAN J LAUFFER PO BOX 969 LIVERMORE CA 94551-0969
1	OAK RIDGE NATL LAB C D WARREN MS 8039 PO BOX 2008 OAK RIDGE TN 37831
4	NIST M VANLANDINGHAM MS 8621 J CHIN MS 8621 J MARTIN MS 8621 D DUTHINH MS 8611 100 BUREAU DR GAITHERSBURG MD 20899
1	HYDROGEOLOGIC INC SERDP ESTCP SPT OFC S WALSH 1155 HERNDON PKWY STE 900 HERNDON VA 20170

NO. OF COPIES	ORGANIZATION
3	NASA LANGLEY RESEARCH CTR AMSRD ARL VS W ELBER MS 266 F BARTLETT JR MS 266 G FARLEY MS 266 HAMPTON VA 23681-0001
1	NASA LANGLEY RESEARCH CTR T GATES MS 188E HAMPTON VA 23661-3400
1	FHWA E MUNLEY 6300 GEORGETOWN PIKE MCLEAN VA 22101
1	USDOT FEDERAL RAILROAD M FATEH RDV 31 WASHINGTON DC 20590
3	CYTEC FIBERITE R DUNNE D KOHLI R MAYHEW 1300 REVOLUTION ST HAVRE DE GRACE MD 21078
1	DIRECTOR NGIC IANG TMT 2055 BOULDERS RD CHARLOTTESVILLE VA 22911-8318
1	SIOUX MFG B KRIEL PO BOX 400 FT TOTTEN ND 58335
2	3TEX CORP A BOGDANOVICH J SINGLETARY 109 MACKENAN DR CARY NC 27511
1	3M CORP J SKILDUM 3M CENTER BLDG 60 IN 01 ST PAUL MN 55144-1000

NO. OF COPIES | ORGANIZATION

1 DIRECTOR
DEFENSE INTLLGNC AGNCY
TA 5
K CRELLING
WASHINGTON DC 20310

1 ADVANCED GLASS FIBER YARNS
T COLLINS
281 SPRING RUN LANE STE A
DOWNINGTON PA 19335

1 COMPOSITE MATERIALS INC
D SHORTT
19105 63 AVE NE
PO BOX 25
ARLINGTON WA 98223

1 JPS GLASS
L CARTER
PO BOX 260
SLATER RD
SLATER SC 29683

1 COMPOSITE MATERIALS INC
R HOLLAND
11 JEWEL CT
ORINDA CA 94563

1 COMPOSITE MATERIALS INC
C RILEY
14530 S ANSON AVE
SANTA FE SPRINGS CA 90670

2 SIMULA
J COLTMAN
R HUYETT
10016 S 51ST ST
PHOENIX AZ 85044

2 PROTECTION MATERIALS INC
M MILLER
F CRILLEY
14000 NW 58 CT
MIAMI LAKES FL 33014

2 FOSTER MILLER
M ROYLANCE
W ZUKAS
195 BEAR HILL RD
WALTHAM MA 02354-1196

NO. OF COPIES | ORGANIZATION

1 ROM DEVELOPMENT CORP
R O MEARA
136 SWINEBURNE ROW
BRICK MARKET PLACE
NEWPORT RI 02840

2 TEXTRON SYSTEMS
T FOLTZ
M TREASURE
1449 MIDDLESEX ST
LOWELL MA 01851

1 O GARA HESS & EISENHARDT
M GILLESPIE
9113 LESAINT DR
FAIRFIELD OH 45014

2 MILLIKEN RESEARCH CORP
H KUHN
M MACLEOD
PO BOX 1926
SPARTANBURG SC 29303

1 CONNEAUGHT INDUSTRIES INC
J SANTOS
PO BOX 1425
COVENTRY RI 02816

1 ARMTEC DEFENSE PRODUCTS
S DYER
85 901 AVE 53
PO BOX 848
COACHELLA CA 92236

1 NATL COMPOSITE CTR
T CORDELL
2000 COMPOSITE DR
KETTERING OH 45420

3 PACIFIC NORTHWEST LAB
M SMITH
G VAN ARSDALE
R SHIPPELL
PO BOX 999
RICHLAND WA 99352

1 SAIC
M PALMER
1410 SPRING HILL RD STE 400
MS SH4 5
MCLEAN VA 22102

NO. OF COPIES	ORGANIZATION
1	ALLIANT TECHSYSTEMS INC 4700 NATHAN LN N PLYMOUTH MN 55442-2512
1	APPLIED COMPOSITES W GRISCH 333 NORTH SIXTH ST ST CHARLES IL 60174
1	CUSTOM ANALYTICAL ENG SYS INC A ALEXANDER 13000 TENSOR LANE NE FLINTSTONE MD 21530
1	AAI CORP DR N B MCNELLIS PO BOX 126 HUNT VALLEY MD 21030-0126
1	OFC DEPUTY UNDER SEC DEFNS J THOMPSON 1745 JEFFERSON DAVIS HWY CRYSTAL SQ 4 STE 501 ARLINGTON VA 22202
3	ALLIANT TECHSYSTEMS INC J CONDON E LYNAM J GERHARD WV01 16 STATE RT 956 PO BOX 210 ROCKET CENTER WV 26726-0210
1	PROJECTILE TECHNOLOGY INC 515 GILES ST HAVRE DE GRACE MD 21078
1	HEXCEL INC R BOE PO BOX 18748 SALT LAKE CITY UT 84118
1	PRATT & WHITNEY C WATSON 400 MAIN ST MS 114 37 EAST HARTFORD CT 06108

NO. OF COPIES	ORGANIZATION
5	NORTHROP GRUMMAN B IRWIN K EVANS D EWART A SHREKENHAMER J MCGLYNN BLDG 160 DEPT 3700 1100 WEST HOLLYVALE ST AZUSA CA 91701
1	HERCULES INC HERCULES PLAZA WILMINGTON DE 19894
1	BRIGS COMPANY J BACKOFEN 2668 PETERBOROUGH ST HERNDON VA 22071-2443
1	ZERNOW TECHNICAL SERVICES L ZERNOW 425 W BONITA AVE STE 208 SAN DIMAS CA 91773
1	GENERAL DYNAMICS OTS L WHITMORE 10101 NINTH ST NORTH ST PETERSBURG FL 33702
2	GENERAL DYNAMICS OTS FLINCHBAUGH DIV K LINDE T LYNCH PO BOX 127 RED LION PA 17356
1	GKN WESTLAND AEROSPACE D OLDS 450 MURDOCK AVE MERIDEN CT 06450-8324
2	BOEING ROTORCRAFT P MINGURT P HANDEL 800 B PUTNAM BLVD WALLINGFORD PA 19086

NO. OF COPIES	ORGANIZATION
5	SIKORSKY AIRCRAFT G JACARUSO T CARSTENSAN B KAY S GARBO MS S330A J ADELMANN 6900 MAIN ST PO BOX 9729 STRATFORD CT 06497-9729
1	AEROSPACE CORP G HAWKINS M4 945 2350 E EL SEGUNDO BLVD EL SEGUNDO CA 90245
2	CYTEC FIBERITE M LIN W WEB 1440 N KRAEMER BLVD ANAHEIM CA 92806
2	UDLP G THOMAS M MACLEAN PO BOX 58123 SANTA CLARA CA 95052
1	UDLP WARREN OFC A LEE 31201 CHICAGO RD SOUTH SUITE B102 WARREN MI 48093
2	UDLP R BRYNSVOLD P JANKE MS 170 4800 EAST RIVER RD MINNEAPOLIS MN 55421-1498
1	LOCKHEED MARTIN SKUNK WORKS D FORTNEY 1011 LOCKHEED WAY PALMDALE CA 93599-2502
1	LOCKHEED MARTIN R FIELDS 5537 PGA BLVD SUITE 4516 ORLANDO FL 32839

NO. OF COPIES	ORGANIZATION
1	NORTHRUP GRUMMAN CORP ELECTRONIC SENSORS & SYSTEMS DIV E SCHOCH MS V 16 1745A W NURSERY RD LINTHICUM MD 21090
1	GDLS DIVISION D BARTLE PO BOX 1901 WARREN MI 48090
2	GDLS D REES M PASIK PO BOX 2074 WARREN MI 48090-2074
1	GDLS MUSKEGON OPER M SOIMAR 76 GETTY ST MUSKEGON MI 49442
1	GENERAL DYNAMICS AMPHIBIOUS SYS SURVIVABILITY LEAD G WALKER 991 ANNAPOLIS WAY WOODBRIDGE VA 22191
6	INST FOR ADVANCED TECH H FAIR I MCNAB P SULLIVAN S BLESS W REINECKE C PERSAD 3925 W BRAKER LN STE 400 AUSTIN TX 78759-5316
1	ARROW TECH ASSOC 1233 SHELBURNE RD STE D8 SOUTH BURLINGTON VT 05403-7700
1	R EICHELBERGER CONSULTANT 409 W CATHERINE ST BEL AIR MD 21014-3613

NO. OF COPIES	ORGANIZATION
1	SAIC G CHRYSSOMALLIS 8500 NORMANDALE LAKE BLVD SUITE 1610 BLOOMINGTON MN 55437-3828
1	UCLA MANE DEPT ENGR IV H T HAHN LOS ANGELES CA 90024-1597
2	UNIV OF DAYTON RESEARCH INST R Y KIM A K ROY 300 COLLEGE PARK AVE DAYTON OH 45469-0168
1	UMASS LOWELL PLASTICS DEPT N SCHOTT 1 UNIVERSITY AVE LOWELL MA 01854
1	IIT RESEARCH CTR D ROSE 201 MILL ST ROME NY 13440-6916
1	GA TECH RESEARCH INST GA INST OF TCHNLGY P FRIEDERICH ATLANTA GA 30392
1	MICHIGAN ST UNIV MSM DEPT R AVERILL 3515 EB EAST LANSING MI 48824-1226
1	UNIV OF WYOMING D ADAMS PO BOX 3295 LARAMIE WY 82071
1	PENN STATE UNIV R S ENGEL 245 HAMMOND BLDG UNIVERSITY PARK PA 16801

NO. OF COPIES	ORGANIZATION
2	PENN STATE UNIV R MCNITT C BAKIS 212 EARTH ENGR SCIENCES BLDG UNIVERSITY PARK PA 16802
1	PURDUE UNIV SCHOOL OF AERO & ASTRO C T SUN W LAFAYETTE IN 47907-1282
1	STANFORD UNIV DEPT OF AERONAUTICS & AEROBALLISTICS S TSAI DURANT BLDG STANFORD CA 94305
1	UNIV OF MAINE ADV STR & COMP LAB R LOPEZ ANIDO 5793 AEWC BLDG ORONO ME 04469-5793
1	JOHNS HOPKINS UNIV APPLIED PHYSICS LAB P WIENHOLD 11100 JOHNS HOPKINS RD LAUREL MD 20723-6099
1	UNIV OF DAYTON J M WHITNEY COLLEGE PARK AVE DAYTON OH 45469-0240
1	NORTH CAROLINA ST UNIV CIVIL ENGINEERING DEPT W RASDORF PO BOX 7908 RALEIGH NC 27696-7908
5	UNIV OF DELAWARE CTR FOR COMPOSITE MTRLS J GILLESPIE M SANTARE S YARLAGADDA S ADVANI D HEIDER 201 SPENCER LAB NEWARK DE 19716

NO. OF COPIES	ORGANIZATION
1	DEPT OF MTRLS SCIENCE & ENGRG UNIV OF ILLINOIS AT URBANA CHAMPAIGN J ECONOMY 1304 WEST GREEN ST 115B URBANA IL 61801
1	UNIV OF MARYLAND DEPT OF AEROSPACE ENGRG A J VIZZINI COLLEGE PARK MD 20742
1	DREXEL UNIV A S D WANG 3141 CHESTNUT ST PHILADELPHIA PA 19104
3	UNIV OF TEXAS AT AUSTIN CTR FOR ELECTROMECHANICS J PRICE A WALLS J KITZMILLER 10100 BURNET RD AUSTIN TX 78758-4497
3	VA POLYTECHNICAL INST & STATE UNIV DEPT OF ESM M W HYER K REIFSNIDER R JONES BLACKSBURG VA 24061-0219
1	SOUTHWEST RESEARCH INST ENGR & MATL SCIENCES DIV J RIEGEL 6220 CULEBRA RD PO DRAWER 28510 SAN ANTONIO TX 78228-0510
1	BATELLE NATICK OPERS B HALPIN 313 SPEEN ST NATICK MA 01760
3	DIRECTOR US ARMY RESEARCH LAB AMSRD ARL WM MB A FRYDMAN 2800 POWDER MILL RD ADELPHI MD 20783-1197

NO. OF COPIES	ORGANIZATION
	ABERDEEN PROVING GROUND
1	US ARMY ATC CSTE DTC AT AC I W C FRAZER 400 COLLERAN RD APG MD 21005-5059
91	DIR USARL AMSRD ARL CI AMSRD ARL O AP EG M ADAMSON AMSRD ARL SL BA AMSRD ARL SL BB D BELY AMSRD ARL WM J SMITH H WALLACE AMSRD ARL WM B A HORST T KOGLER AMSRD ARL WM BA D LYON AMSRD ARL WM BC J NEWILL P PLOSTINS A ZIELINSKI AMSRD ARL WM BD P CONROY B FORCH M LEADORE C LEVERITT R LIEB R PESCE RODRIGUEZ B RICE AMSRD ARL WM BF S WILKERSON AMSRD ARL WM M B FINK J MCCAULEY AMSRD ARL WM MA L GHIORSE S MCKNIGHT E WETZEL AMSRD ARL WM MB J BENDER T BOGETTI L BURTON R CARTER K CHO W DE ROSSET G DEWING R DOWDING W DRYSDALE

NO. OF COPIES	ORGANIZATION
	R EMERSON D HENRY D HOPKINS R KASTE L KECSKES M MINNICINO B POWERS D SNOHA J SOUTH M STAKER J SWAB J TZENG AMSRD ARL WM MC J BEATTY R BOSSOLI E CHIN S CORNELISON D GRANVILLE B HART J LASALVIA J MONTGOMERY F PIERCE E RIGAS W SPURGEON AMSRD ARL WM MD B CHEESEMAN P DEHMER R DOOLEY G GAZONAS S GHIORSE C HOPPEL M KLUSEWITZ W ROY J SANDS D SPAGNUOLO S WALSH S WOLF AMSRD ARL WM RP J BORNSTEIN C SHOEMAKER AMSRD ARL WM T B BURNS AMSRD ARL WM TA W BRUCHEY M BURKINS W GILLICH B GOOCH T HAVEL E HORWATH M NORMANDIA J RUNYEON M ZOLTOSKI

NO. OF COPIES	ORGANIZATION
	AMSRD ARL WM TB P BAKER AMSRD ARL WM TC R COATES AMSRD ARL WM TD D DANDEKAR T HADUCH T MOYNIHAN M RAFTENBERG S SCHOENFELD T WEERASOORIYA AMSRD ARL WM TE A NIILER J POWELL

NO. OF COPIES	ORGANIZATION
1	LTD R MARTIN MERL TAMWORTH RD HERTFORD SG13 7DG UK
1	SMC SCOTLAND P W LAY DERA ROSYTH ROSYTH ROYAL DOCKYARD DUNFERMLINE FIFE KY 11 2XR UK
1	CIVIL AVIATION ADMINSTRATION T GOTTESMAN PO BOX 8 BEN GURION INTRNL AIRPORT LOD 70150 ISRAEL
1	AEROSPATIALE S ANDRE A BTE CC RTE MD132 316 ROUTE DE BAYONNE TOULOUSE 31060 FRANCE
1	DRA FORT HALSTEAD P N JONES SEVEN OAKS KENT TN 147BP UK
1	SWISS FEDERAL ARMAMENTS WKS W LANZ ALLMENDSTRASSE 86 3602 THUN SWITZERLAND
1	DYNAMEC RESEARCH LAB AKE PERSSON BOX 201 SE 151 23 SODERTALJE SWEDEN

NO. OF COPIES	ORGANIZATION
1	ISRAEL INST OF TECHLGY S BODNER FACULTY OF MECHANICAL ENGR HAIFA 3200 ISRAEL
1	DSTO WEAPONS SYSTEMS DIVISION N BURMAN RLLWS SALISBURY SOUTH AUSTRALIA 5108 AUSTRALIA
1	DEF RES ESTABLISHMENT VALCARTIER A DUPUIS 2459 BLVD PIE XI NORTH VALCARTIER QUEBEC CANADA PO BOX 8800 COURCELETTE GOA IRO QUEBEC CANADA
1	ECOLE POLYTECH J MANSON DMX LTC CH 1015 LAUSANNE SWITZERLAND
1	TNO DEFENSE RESEARCH R IJSSELSTEIN ACCOUNT DIRECTOR R&D ARMEE PO BOX 6006 2600 JA DELFT THE NETHERLANDS
2	FOA NATL DEFENSE RESEARCH ESTAB DIR DEPT OF WEAPONS & PROTECTION B JANZON R HOLMLIN S 172 90 STOCKHOLM SWEDEN

NO. OF COPIES	ORGANIZATION
2	DEFENSE TECH & PROC AGENCY GROUND I CREWTHER GENERAL HERZOG HAUS 3602 THUN SWITZERLAND
1	MINISTRY OF DEFENCE RAFAEL ARMAMENT DEVELOPMENT AUTH M MAYSELESS PO BOX 2250 HAIFA 31021 ISRAEL
1	TNO DEFENSE RESEARCH I H PASMAN POSTBUS 6006 2600 JA DELFT THE NETHERLANDS
1	B HIRSCH TACHKEMONY ST 6 NETAMUA 42611 ISRAEL
1	DEUTSCHE AEROSPACE AG DYNAMICS SYSTEMS M HELD PO BOX 1340 D 86523 SCHROBENHAUSEN GERMANY

INTENTIONALLY LEFT BLANK.